Catalysis Communications 162 (2022) 106383

Contents lists available at ScienceDirect

Catalysis Communications

journal homepage: www.elsevier.com/locate/catcom

Short communication

# Iron-chromium mixed metal oxides catalyse the oxidative dehydrogenation of propane using carbon dioxide

Tongqi Ye [a,*], James H. Carter [b,*], Bao Chen [a], Xin Li [a], Yuewen Ye [a], Stuart H. Taylor [b], Graham J. Hutchings [b]

[a] School of Chemistry and Chemical Engineering, Hefei University of Technology, Hefei, Anhui 230009, PR China
[b] Max Planck-Cardiff Centre on the Fundamentals of Heterogeneous Catalysis FUNCAT, Cardiff Catalysis Institute, School of Chemistry, Cardiff University, Main Building, Park Place, Cardiff CF10 3AT, UK

ARTICLE INFO

*Keywords:*
Propane dehydrogenation
Propene
Carbon dioxide
Soft oxidation
Chromium oxide
Iron oxide

ABSTRACT

The oxidative dehydrogenation of propane to propene using carbon dioxide is an attractive novel synthesis route to produce a key platform chemical. We investigated iron-chromia catalysts prepared by sol-gel. The mixed oxides showed improved specific surface area and a high concentration of acid and base sites and were found to be highly active catalysts. Although coking was observed over the catalysts, oxidative regeneration restored the majority of the initial activity over 5 consecutive cycles. The initial space time yield was amongst the most active Cr-based catalysts in the literature.

## 1. Introduction

Propene is a major platform chemical and precursor to many chemicals and materials, most significantly polypropene. Worldwide annual propene production was 130 megatonnes in 2019 and it is predicted that demand will increase over the next decade [1]. Current production methods mostly rely on steam and fluid-catalysed cracking technologies, which have several drawbacks: Cracking of naphtha produces propane as one of several products, meaning the atom economy is low. Additionally, the demand for propene has been expected to outstrip supply, hence the emergence of the 'propene gap'. In order to fill this gap, industry has responded by investing in 'on-purpose' propene production processes, namely the direct dehydrogenation of propane (DDH), shown in Eq. (1).

$$C_3H_8 \rightleftharpoons C_3H_6 + H_2 \quad (1)$$

To date there are several commercial processes in operation, including Oleflex, Dow FCdh, STAR process, CATOFIN and K-PRO. In most cases, Pt- or Cr-based catalysts are employed. While selectivity above 90% can be achieved at conversions in excess of 40%, there are also disadvantages associated with this method of propene production. Coking remains a challenge in all cases, and frequent catalyst regeneration cycles are needed, which involves burning off coke. Secondly, the reaction is equilibrium-limited and so operating conditions, and ultimately $C_3H_6$ yields, are restricted.

The oxidative dehydrogenation of propane to propene using carbon dioxide (ODH-$CO_2$) represents an interesting alternative to direct dehydrogenation: The addition of $CO_2$ offers a strategy to utilise carbon, which could have a significant effect on the carbon neutrality in the life cycle of propene production [2]. $CO_2$ facilitates the reverse water-gas shift reaction (RWGS, Eq. (2)) to remove $H_2$ and form $H_2O$, which means higher equilibrium yields of propene are possible. Furthermore, the reverse Boudouard reaction (Eq. (3)) can take place, which in turn removes coke and extends the catalyst lifetime.

$$CO_2 + H_2 \rightleftharpoons CO + H_2O \quad (2)$$

$$CO_2 + C \rightleftharpoons 2CO \quad (3)$$

For the above reasons, ODH-$CO_2$ has attracted significant academic interest in the last 20 years. The most active catalysts reported to date are mixed metal oxide-based catalysts that use Cr or Ga oxides as the active component. Notably, Michorczyk and co-workers have made several contributions to the field and reported numerous supported $CrO_x$ catalysts with promising performance [3–5]. In all cases, deactivation via coking was a challenge. In addition to Cr, $Ga_2O_3/Al_2O_3$ [6,7], $Fe_2O_3$ [8], $In_2O_3$ [9] and various other supported transition and platinum group metals have been reported as active catalysts [10,11].

Generally, supports for Cr-based catalysts are inert and most often

* Corresponding authors.
*E-mail addresses:* yetq@hfut.edu.cn (T. Ye), carterj5@cardiff.ac.uk (J.H. Carter).

https://doi.org/10.1016/j.catcom.2021.106383
Received 3 November 2021; Received in revised form 10 December 2021; Accepted 17 December 2021
Available online 17 December 2021
1566-7367/© 2021 The Authors. Published by Elsevier B.V. This is an open access article under the CC BY license (http://creativecommons.org/licenses/by/4.0/).

**Table 1**
Physical and chemical properties of FeCr catalysts.

| Sample | $S_{BET}$ ($m^2$ $g^{-1}$) | Average crystallite size[c] (nm) | Relative acid sites[d] | Relative basic sites[d] |
|---|---|---|---|---|
| FeCr0 | 8.5 | 40 | 9 | 67 |
| FeCr25 | 20 | 18 | 23 | 5 |
| FeCr50 | 29 | 5.9 | 39 | 20 |
| FeCr75 | 15 | 33 | 21 | 6 |
| FeCr100 | 23 | 75 | 3 | 3 |

[a]Specific surface area determined by BET method. Particle diameter, [c]Calculated by the Scherrer equation. [d]Based on mass normalised, uncalibrated integrated areas under $NH_3$-TPD and $CO_2$-TPD traces (Figs. S2a and b).

they are $SiO_2$-based. The main limitation in the field of ODH-$CO_2$ is the low conversion and $C_3H_6$ yields compared to optimised DDH reactions. Therefore, the discovery of novel, highly active catalysts is of interest. The main mechanistic difference between DDH and ODH-$CO_2$ is the requirement of the catalyst to activate $CO_2$ and facilitate the reverse water-gas shift reaction. While $Cr_2O_3$ is highly active in the DDH reaction, it's activity as a reverse water-gas shift catalyst may not be sufficiently high. Mixed metal oxides of Cr and Fe are applied as high-temperature water-gas shift catalysts and consequently may be interesting candidates for ODH-$CO_2$ catalysts. In this work, we investigate this hypothesis by preparing a range of FeCr mixed oxides and testing them for DDH and ODH-$CO_2$.

## 2. Results and discussion

### 2.1. Catalyst characterisation

A series of $FeCrO_x$ catalysts were prepared using a typical sol-gel technique (experimental details provided in the Supplementary Information), with various Cr:Fe molar ratios. The catalysts are referred to as FeCrX, where $X = mol_{Cr} / (mol_{Cr} + mol_{Fe}) \times 100$. For example, FeCr25 is a mixed metal oxide where there is 25 mol% Cr and 75 Fe mol%. For simplicity, the Fe- and Cr-only oxides are simply referred to as Fe or Cr. The series of catalysts was initially analysed by ICP-AES to measure the actual ratio of Fe:Cr. The results are presented in Table S1 and are in excellent agreement with the nominal values, showing that the sol-gel method is appropriate to prepare mixed FeCr oxide catalysts.

The catalysts were then characterised to understand how the addition of Fe to $CrO_x$ affects the physical and chemical properties. Table 1 shows that the specific surface area varies substantially with the molar ratio of Fe:Cr. The highest surface area, 29 $m^2$ $g^{-1}$, was observed over the $Fe_{0.5}Cr_{0.5}O_x$ catalyst. FeCr100 and FeCr0 showed values of 8.5 and 23 $m^2$ $g^{-1}$, respectively. XRD patterns of the catalysts are presented in Fig. S1. Typical diffraction patterns indicative of $Fe_2O_3$ and $Cr_2O_3$ were observed, with principal reflections at 24, 34 and 37° [12,13]. In the case of Cr, the reflections were observed at a higher angle (2θ), consistent with smaller lattice spacings in the crystal structure. The mixed metal oxides were clearly less crystalline than the Cr and Fe catalysts, which is also consistent with the higher specific surface areas observed

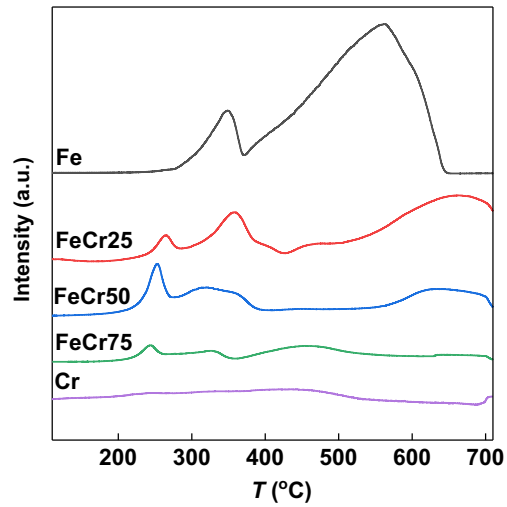


**Fig. 1.** $H_2$-TPR profiles of the FeCr catalysts.

in these samples. In the case of FeCr25 and FeCr50, there is a broad, but visible additional reflection at 31 and 42°. The crystallite size was estimated using the Scherrer equation (Table 1) and is inversely proportional to the specific surface areas of the FeCr oxides. $Cr_2O_3$ is the outlier, which shows a reasonable specific surface area but a larger crystallite size.

It is well known that acid and base sites play an important role in DDH and ODH-$CO_2$ catalysis. Acid sites are able to activate $C_3H_8$, but if too strong, can promote deep dehydrogenation and coke formation [2]. Basic sites have also been implicated in coke formation over $Zn/ZrO_2$ catalysts [14], but are generally considered to be sites for $CO_2$ activation. Accordingly, the balance of these sites can influence the surface concentration of $C_3H_8$, $CO_2$ and the rate of dehydrogenation and RWGS. $NH_3$-TPD and $CO_2$-TPD analysis was therefore completed on each sample in order to establish the concentration and strength of the acid and base sites present (Fig. S2). In poorly acidic and basic samples, the interpretation of the data is challenging due to the low intensity of desorption peaks. However, there are clear differences in the profiles of each sample. In general, the mixed oxides had more acid and basic sites than the Fe and Cr. Regarding the acid sites, the mixed metal oxide catalyst exhibited two broad desorption peaks, centred approximately at 200 and 380 °C. Fe and Cr exhibited lower $NH_3$ desorption, although FeCr100 showed a high temperature desorption peak at 550 °C, indicative of a strong Lewis or Bronsted acid site. The $CO_2$-TPD profiles also show an increase in the intensity of the desorption peaks, indicative of an increase in the number of basic sites on the catalyst surface. The FeCr50 exhibited the largest desorption peaks in the series of catalysts. As the sample mass was controlled in each experiment, the integrated area of the peaks gives allows the relative concentration of acid and base sites on the catalysts to be inferred. These estimations are presented in Table 2. This shows that FeCr50 has the highest concentration of acid

**Table 2**
DDH and ODH-$CO_2$ results for the $FeCrO_x$ catalysts.

| Sample | DDH | | | | | | ODH-$CO_2$ | | | | | |
|---|---|---|---|---|---|---|---|---|---|---|---|---|
| | Conv. (%) | Selectivity (%) | | | $C_3$ yield (%) | C balance[b] (%) | Conv. (%) | Selectivity (%) | | | $C_3$ yield (%) | C balance[b] (%) |
| | | $C_3$ | $C_1$ | Others[a] | | | | $C_3$ | $C_1$ | Others[a] | | |
| Fe | 5.4 | 37.9 | 0.9 | 10.6 | 2.0 | 49 | 7.7 | 35.1 | 1.1 | 7.7 | 2.7 | 44 |
| FeCr25 | 7.3 | 51.7 | 1.8 | 9.5 | 3.8 | 63 | 10.8 | 64.2 | 12.7 | 5.4 | 6.9 | 82 |
| FeCr50 | 9.1 | 68.2 | 2.9 | 6.8 | 6.2 | 78 | 14.2 | 71 | 17.9 | 5.3 | 10.1 | 94 |
| FeCr75 | 6.5 | 76.9 | 2.7 | 5.5 | 5.0 | 85 | 9.4 | 77.5 | 10.4 | 7.3 | 7.3 | 95 |
| Cr | 3.2 | 78.2 | 2.7 | 10.3 | 2.5 | 91 | 4.6 | 77.5 | 7.5 | 13.9 | 3.6 | 99 |

[a] Others refers to sum of $C_2H_4$ and $C_2H_6$.
[b] C balance = Converted Carbon balance.

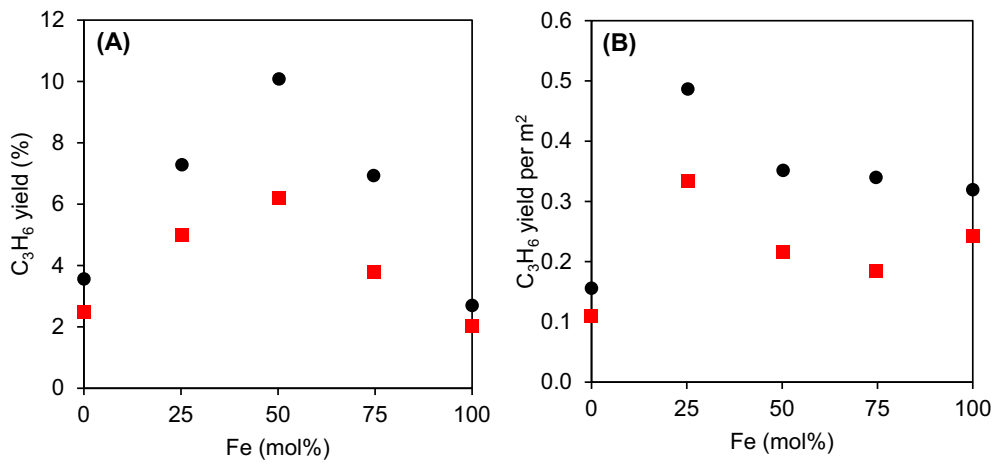


**Fig. 2.** (A) The relationship between Fe:Cr ratio and the $C_3H_6$ yield and (B) the relationship between the Fe:Cr ratio and the surface area normalised $C_3H_6$ yields in the DDH (■) and ODH-$CO_2$ (•) reactions.

and basic sites out of the series of samples.

SEM analysis was carried out to probe the morphology of the prepared catalysts. Representative micrographs are presented in Fig. S3(a-e). The morphology of the Fe, Cr and FeCr25 (a,b and e) show small, dense clusters of particles around 20 nm in diameter. Conversely, the FeCr50 and FeCr75 samples (c and d) are bimodal in their particle size distribution. There are very large particles in the order of several hundred nanometres in size, with small particles below 20 nm decorating the edges.

In order to probe the redox properties of the catalysts, $H_2$-TPR was carried out (Fig. 1). The reduction profile of Fe is defined by two peaks, one at 350 °C and one around 550 °C. The first peak is the reduction of hematite, $Fe_2O_3$ to magnetite, $Fe_3O_4$. The higher temperature peak is due to the complete reduction of magnetite to $Fe^0$ [15]. The addition of Cr causes a significant shift to lower temperatures in these peaks, to 255 and 360 °C. This indicates that the introduction of Cr enhances the reducibility of the catalyst. The reducibility of bulk $Cr_2O_3$ compared to $Fe_2O_3$ is very poor and indicates that the addition of Fe to Cr introduces redox active sites. The dissociative activation of $CO_2$ can take place at oxygen vacancies, therefore the increased reducibility of the FeCr catalysts would be expected to facilitate more facile $CO_2$ activation than Fe or Cr.

### 2.2. Propane dehydrogenation

The series of catalysts were evaluated in the DDH and ODH-$CO_2$ reactions. It has been shown that for some catalysts the addition of $CO_2$ inhibits propane activation, hence the value in comparing DDH and ODH-$CO_2$ activity [16–18]. The origin of this inhibition effect was determined by Xu et al. to be due to $CO_2$ blocking propane adsorption on basic sites [16]. The effect is support-dependent and underlines the importance of balancing acid and base sites on the catalyst surface. Table 2 shows the initial conversion and selectivity of the catalysts in the DDH and ODH-$CO_2$ reactions.

There are several notable differences in the performance of the catalysis in the presence and absence of $CO_2$. It is clear that the combination of Fe and Cr leads to higher activity in both reactions. When the conversion and $C_3H_6$ yield are plotted as a function of the Fe:Cr ratio, a clear volcano plot is observed with the maximum at the FeCr50 catalyst (Fig. 2a). When normalised for differences in specific surface area (Fig. 2b), a trend is still observed, whereby the mixed FeCr catalysts are more active than the Fe or Cr-only catalysts. Across the range of catalysts, the yield varied by more than a factor of 2, which indicates other differences beyond surface area in the properties of the catalyst contributed to the differences in activity. The relationship between acid/base sites and $C_3H_6$ yield was also investigated. Fig. S4a shows that there is a positive correlation between the $C_3H_6$ yield per $m^2$ and the acid sites per $m^2$. Fig. S4b shows that there is a volcano-type relationship between the surface area normalised $C_3H_6$ yield and the number of basic sites per $m^2$. As discussed above, acid sites are considered to be activation sites for $C_3H_8$ molecules, and so it is expected that there would be such a correlation. $CO_2$ activation takes place on basic sites and so it would be expected that more basic sites would lead to higher yields of $C_3H_6$. The correlation in Fig. S4b suggests that the reaction is not limited by $CO_2$ activation, rather it is limited by $C_3H_8$ activation. The catalysts with the highest concentration of basic sites have an intermediate concentration of acid sites, and an intermediate $C_3H_6$ yield. Therefore the improved performance of the mixed FeCr catalysts is most likely due to the facilitation of more active sites for $C_3H_8$ activation.

The addition of $CO_2$ to these catalysts is clearly beneficial. The $C_3H_6$ yield increases across all catalysts, but to the largest extent over the mixed metal oxide catalysts, suggesting that the mixed metal oxides can efficiently activate $CO_2$ and $C_3H_8$. A further benefit of $CO_2$ is the improved converted carbon balance. In the DDH reaction, the converted carbon balance improves with the addition of Fe, but in the most active catalyst (FeCr50), it is only 78%. In the ODH-$CO_2$ reaction, the carbon balance also improves as Fe content increases, but above 50 mol% Fe, the converted carbon balance reaches 94% and above. The missing carbon may be ascribed to deep dehydrogenation forming coke on the catalyst. It has been shown that dry reforming can occur over supported nanoparticle catalysts and so this pathway cannot be disregarded [11]. Additionally, it is not possible to distinguish between dry reforming, steam reforming and the reverse Boudouard reaction. Unfortunately, quantification of CO, $CO_2$ and $H_2$ was not possible using the current analysis, and therefore the rate of CO formation or deep dehydrogenation to coke cannot be determined.It should be noted that the selectivity calculations are based on the moles of converted carbon, therefore are not impacted by the inability to quantify CO or coke formation.

$C_3H_6$ selectivity also increases as Fe content increases, but values are modestly improved in the presence of $CO_2$. Aside from $C_3H_6$, $CH_4$ and some $C_2$ products ($C_2H_4$ and $C_2H_6$) were also formed. Interestingly, the $CH_4$ formation was much higher in the presence of $CO_2$, which is likely due to methanation of $CO_2$ and CO (Eqs. (4) and (5)). Cracking (Eq. (6)) or hydrogenolysis (Eq. (7)) reactions are generally suggested to be responsible for $CH_4$ and $C_2H_4$ formation in DDH, but $C_2H_4$ may react further over the catalyst *via* deep dehydrogenation to form coke, hence the deviation of $CH_4$ and $C_2H_4$ from stoichiometric values.

$$CO_2 + 4H_2 \rightarrow CH_4 + 2H_2O \quad (4)$$

$$CO + 3H_2 \rightarrow CH_4 + H_2O \quad (5)$$

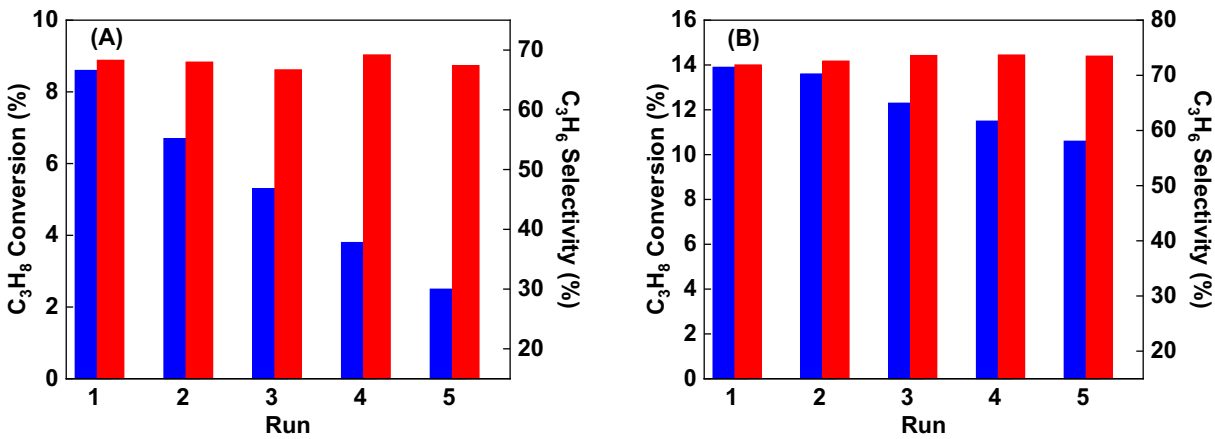


**Fig. 3.** Catalytic cycles of FeCr50 under DDH (A) and ODH-$CO_2$ (B) reaction conditions. Blue bar: $C_3H_8$ conversion, red bar: $C_3H_6$ selectivity. (For interpretation of the references to colour in this figure legend, the reader is referred to the web version of this article.)

$$C_3H_8 + H_2 \rightarrow CH_4 + C_2H_6 \quad (6)$$

$$C_3H_8 \rightarrow CH_4 + C_2H_4 \quad (7)$$

The stability of a catalyst is of prime importance in evaluating its performance. Fig. S5(a-d) shows the time-on-stream activity of the catalysts over 2 h. In the DDH reaction, the conversion of all the catalysts reaches 0% after 2 h. This rapid deactivation is most likely caused by coking of the catalyst from deep dehydrogenation, as is widely reported for DDH [2]. The propene selectivity increases on-stream as conversion drops, as is often observed in dehydrogenation reactions. In the ODH-$CO_2$ reaction, the catalysts are clearly more stable, but still deactivate quite rapidly. The most active catalyst, FeCr50, retained only 33% of its initial activity after 2 h on-stream, but still maintained the highest conversion of the series of catalysts after this time, on par with FeCr25. Similarly, the propene selectivity increases on-stream as the conversion decreases.

It is well known that even commercial DDH catalysts require frequent regeneration cycles to operate efficiently. Therefore, the ability to recover activity after regeneration is an additional indicator of long-term stability. Fig. 3 shows the performance of the most active catalyst, FeCr50, after 5 consecutive reaction cycles. The regeneration step involved switching the reaction feed to flowing air for 2 h, purging with $N_2$ and then switching back to the DDH reaction mixture, as described in the Supplementary Information. In the DDH cycles, the $C_3H_8$ conversion quickly decreases after regeneration, falling from 8.5% in the first run, to 2.5% in the fifth run and the $C_3H_6$ selectivity remains constant throughout each run. In the ODH-$CO_2$ cycles, the $C_3H_8$ conversion decreases from 14% to 10.5% after 5 runs, a more modest deactivation. As was the case for the DDH cycles, the $C_3H_6$ selectivity remains fairly constant and may increase slightly, from 72% to 74%. Clearly, the presence of $CO_2$ enables the catalyst to be regenerated more easily, although the deactivation is not completely reversible. In addition to coking, loss of active surface area through sintering is possible, and this could also occur during the exothermic regeneration step.

Finally, the space time yield of the FeCr catalysts was compared with similar Cr-based ODH-$CO_2$ catalysts. A comparison of these is provided in Table S2 and indicates that FeCr50 is amongst the most active Cr-based catalysts reported for the ODH-$CO_2$ reaction. The most active catalysts in the table are typically supported on high surface area supports, whereas in the current work the catalyst was prepared as a bulk oxide. Supported FeCr catalysts would therefore be of interest to study, but the structural complexity would warrant a full investigation. Specifically, Cr speciation (monomeric, oligomeric, nanocrystalline $Cr_2O_3$) is well known to affect activity and selectivity in $C_3H_8$ dehydrogenation, and the interaction of Fe with such species may be complex.

## 3. Conclusions

The combination of iron and chromium to form mixed metal oxides has been shown to produce highly active and selective ODH-$CO_2$ catalysts. The binary oxides were shown to be more active than either Fe- or Cr-only, partly due to the increased specific surface area of the samples facilitating a higher active surface area. However, the improved selectivity of the catalysts and suppression of coke formation points to an intrinsic improvement in the efficiency of the catalyst. The improved reducibility of the catalysts may play an important role in facilitating $CO_2$ activation (and RWGS) during the reaction, which improved the $C_3H_6$ yield. Additionally, the increase in acid site density may contribute to the improved performance. The FeCr50 catalyst exhibited improved stability compared to Cr-only, and is amongst the most active Cr-based catalysts reported to date. This work highlights the potential of multi-component redox active metal oxides to catalyse the ODH-$CO_2$ reaction, and shows that RWGS catalysts may be considered for ODH-$CO_2$ catalysis, Further optimisation of the catalyst structure and formulation is important to realise the potential of FeCr catalysts for this reaction.

## Declaration of Competing Interest

None.

## Acknowledgements

The authors wish to acknowledge the China Scholarship Council (CSC) Grant #201806695008 and Hefei Municipal Natural Science Foundation (2021043) for funding.

## Appendix A. Supplementary data

Supplementary data to this article can be found online at https://doi.org/10.1016/j.catcom.2021.106383.

## References

[1] Global Data, Global Propylene Capacity and Capital Expenditure Outlook to 2030 – Asia and Middle East to Lead Globally in Terms of Propylene Capacity Additions. https://store.globaldata.com/report/gdch0067mar–global-propylene-capacity-and-capital-expenditure-outlook-to-2030-asia-and-middle-east-to-lead-globally-in-terms-of-propylene-capacity-additions/, 2021 accessed May 4, 2021.

[2] J.H. Carter, T. Bere, J.R. Pitchers, D.G. Hewes, B.D. Vandegehuchte, C.J. Kiely, S. H. Taylor, G.J. Hutchings, Direct and oxidative dehydrogenation of propane: from catalyst design to industrial application, Green Chem. (2021), https://doi.org/10.1039/D1GC03700E.

[3] P. Michorczyk, J. Ogonowski, K. Zeńczak, Activity of chromium oxide deposited on different silica supports in the dehydrogenation of propane with $CO_2$ - a

comparative study, J. Mol. Catal. A Chem. 349 (2011) 1–12, https://doi.org/10.1016/j.molcata.2011.08.019.

[4] P. Michorczyk, K. Zeńczak-Tomera, B. Michorczyk, A. Węgrzyniak, M. Basta, Y. Millot, L. Valentin, S. Dzwigaj, Effect of dealumination on the catalytic performance of Cr-containing Beta zeolite in carbon dioxide assisted propane dehydrogenation, J. CO2 Util. 36 (2020) 54–63, https://doi.org/10.1016/j.jcou.2019.09.018.

[5] P. Michorczyk, J. Ogonowski, P. Kuśtrowski, L. Chmielarz, Chromium oxide supported on MCM-41 as a highly active and selective catalyst for dehydrogenation of propane with $CO_2$, Appl. Catal. A Gen. 349 (2008) 62–69, https://doi.org/10.1016/j.apcata.2008.07.008.

[6] P. Michorczyk, K. Góra-Marek, J. Ogonowski, Dehydrogenation of propane in the presence and absence of $CO_2$ over β-$Ga_2O_3$ supported chromium oxide catalysts, Catal. Lett. 109 (2006) 195–198, https://doi.org/10.1007/s10562-006-0077-z.

[7] M. Chen, J. Xu, F.Z. Su, Y.M. Liu, Y. Cao, H.Y. He, K.N. Fan, Dehydrogenation of propane over spinel-type gallia-alumina solid solution catalysts, J. Catal. 256 (2008) 293–300, https://doi.org/10.1016/j.jcat.2008.03.021.

[8] P. Michorczyk, P. Kuśtrowski, L. Chmielarz, J. Ogonowski, Influence of redox properties on the activity of iron oxide catalysts in dehydrogenation of propane with $CO_2$, React. Kinet. Catal. Lett. 82 (2004) 121–130, https://doi.org/10.1023/B:REAC.0000028813.14758.ea.

[9] M. Chen, J. Xu, Y. Cao, H.Y. He, K.N. Fan, J.H. Zhuang, Dehydrogenation of propane over $In_2O_3$-$Al_2O_3$ mixed oxide in the presence of carbon dioxide, J. Catal. 272 (2010) 101–108, https://doi.org/10.1016/j.jcat.2010.03.007.

[10] E. Nowicka, C. Reece, S.M. Althahban, K.M.H. Mohammed, S.A. Kondrat, D. J. Morgan, Q. He, D.J. Willock, S. Golunski, C.J. Kiely, G.J. Hutchings, Elucidating the role of $CO_2$ in the soft oxidative dehydrogenation of propane over ceria-based catalysts, ACS Catal. 8 (2018) 3454–3468, https://doi.org/10.1021/acscatal.7b03805.

[11] E. Gomez, S. Kattel, B. Yan, S. Yao, P. Liu, J.G. Chen, Combining $CO_2$ reduction with propane oxidative dehydrogenation over bimetallic catalysts, Nat. Commun. 9 (2018) 1398, https://doi.org/10.1038/s41467-018-03793-w.

[12] P.G. Ivanov, S.M. Watts, D.M. Lind, Epitaxial growth of thin films by chemical-vapor deposition from a precursor, J. Appl. Phys. 89 (2001) 1035, https://doi.org/10.1063/1.1331343.

[13] R. Wahab, F. Khan, A.A. Al-Khedhairy, Hematite iron oxide nanoparticles: apoptosis of myoblast cancer cells and their arithmetical assessment, RSC Adv. 8 (2018) 24750–24759, https://doi.org/10.1039/c8ra02613k.

[14] S. Han, D. Zhao, T. Otroshchenko, H. Lund, U. Bentrup, V.A. Kondratenko, N. Rockstroh, S. Bartling, D.E. Doronkin, J.-D. Grunwaldt, U. Rodemerck, D. Linke, M. Gao, G. Jiang, E.V. Kondratenko, Elucidating the nature of active sites and fundamentals for their creation in Zn-containing $ZrO_2$–based catalysts for nonoxidative propane dehydrogenation, ACS Catal. 10 (2020) 8933–8949, https://doi.org/10.1021/ACSCATAL.0C01580.

[15] W.K. Jozwiak, E. Kaczmarek, T.P. Maniecki, W. Ignaczak, W. Maniukiewicz, Reduction behavior of iron oxides in hydrogen and carbon monoxide atmospheres, Appl. Catal. A Gen. 326 (2007) 17–27, https://doi.org/10.1016/J.APCATA.2007.03.021.

[16] B. Xu, B. Zheng, W. Hua, Y. Yue, Z. Gao, Support effect in dehydrogenation of propane in the presence of $CO_2$ over supported gallium oxide catalysts, J. Catal. 239 (2006) 470–477, https://doi.org/10.1016/j.jcat.2006.02.017.

[17] J. Guo, H. Lou, H. Zhao, L. Zheng, X. Zheng, Dehydrogenation and aromatization of propane over rhenium-modified HZSM-5 catalyst, J. Mol. Catal. A Chem. 239 (2005) 222–227, https://doi.org/10.1016/j.molcata.2005.06.019.

[18] I. Takahara, M. Saito, Promoting effects of carbon dioxide on dehydrogenation of propane over a $SiO_2$-supported $Cr_2O_3$ catalyst, Chem. Lett. (1996) 973–974, https://doi.org/10.1246/cl.1996.973.